Using tripodal alcohols to build high-spin molecules and single-molecule magnets

Euan K. Brechin*

Received (in Cambridge, UK) 15th July 2005, Accepted 18th August 2005
First published as an Advance Article on the web 27th September 2005
DOI: 10.1039/b510102f

The combination of tripodal alcohols with paramagnetic 3d transition metal ions leads to the isolation of a host of new clusters, high spin molecules and single-molecule magnets ranging in nuclearity from two to thirty-two.

The synthesis and characterisation of polynuclear clusters of paramagnetic metal ions has attracted intense study since the discovery that such molecules can display the phenomenon of single-molecule magnetism.[1] In these molecules there exists an energy barrier to the relaxation of the magnetisation due to the combination of a large ground state spin multiplicity and a significant negative zero-field splitting of that ground state. This imparts a molecular magnetic memory effect that can be observed as temperature and sweep rate dependent hysteresis loops in single crystal *M vs. H* studies.[2]

Single-Molecule Magnets (SMMs) have many potential applications including high density information storage in which each bit of information is stored as the magnetisation orientation of an individual molecule, and as qubits for quantum computation where the required arbitrary superposition of quantum states with opposite projections of spin are produced by either quantum tunnelling of the magnetization (QTM), inter-molecular exchange, or multi-frequency EPR pulses.[3] Single-molecule magnetism spans areas as diverse as physics, theoretical chemistry, spectroscopy, materials chemistry and synthetic coordination chemistry, as demonstrated by the several hundred papers published on the topic over the last ten years—an effort which has led to the thorough description of the magnetic and electronic structure of several SMMs through the use of techniques as diverse as HF-EPR,[4] NMR,[5] INS,[6] MCD[7] and DFT.[8]

There are now several species displaying such behaviour, the majority of which are transition metal clusters containing Mn ions, since Mn clusters often display large spin ground states and large and negative magneto-anisotropies associated with the presence of Jahn–Teller distorted Mn^{III} ions.[9] However this 'family' of compounds has been extended to various other metals including iron, vanadium, cobalt, nickel[10] and, very recently, combinations of 3d with 4d,[11] 5d[12] and 4f[13] paramagnetic ions, and homometallic Ln^{III} species.[14] To this end two successful, but somewhat opposing, synthetic strategies have been employed. The first is the use of rigid bridging ligands (*e.g.* cyanide) that impose the geometry on the resultant cluster and the second is the use of flexible ligands (*e.g.* carboxylates) that impose little or no geometry.[15] Both approaches have produced beautiful molecules with extremely large spin ground states—$S = 39/2$ for the former[16] and $S \geqslant 23$ and $S = 51/2 \pm 1$ for the latter.[17]

Here we describe some of our efforts toward the preparation of such metal clusters using tripodal alcohol ligands.

School of Chemistry, The University of Edinburgh, West Mains Road, Edinburgh, UK EH9 3JJ. E-mail: ebrechin@staffmail.ed.ac.uk; Tel: +44 (0)131-650-7545

Euan Brechin

Euan Brechin was born in Greenock, Scotland in 1972. He completed both his BSc (1994) and PhD (1997) degrees at The University of Edinburgh (UK), the latter under the supervision of Dr R. E. P. Winpenny. After post-doctoral work with Professor George Christou at Indiana University (USA) he was awarded a Lloyd's of London Tercentenary Foundation Fellowship at the University of Manchester (UK). In 2003 he was awarded an EPSRC Advanced Fellowship at the same institution, before moving to his present position at The University of Edinburgh in September 2004.

Tripodal alcohol ligands

Tripodal ligands such as 1,1,1-tris(hydroxymethyl)ethane (H_3thme, Scheme 1), 1,1,1-tris(hydroxymethyl)propane (H_3tmp) and pentaerythritol (H_4peol) have previously been used in the synthesis of oxo-vanadium and oxo-molybdenum clusters,[18] but until recently, rarely in the synthesis of paramagnetic 3d transition metal clusters.[19]

The basic, though perhaps over-simplistic, principle here is that paramagnetic metal ions linked together into triangular

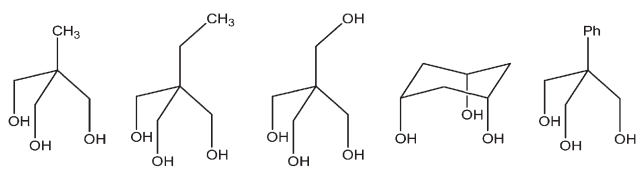

Scheme 1 The tripodal ligands (left to right) 1,1,1- tris(hydroxymethyl)ethane, H_3thme; 1,1,1-tris(hydroxymethyl)propane, H_3tmp; pentaerythritol, H_4peol, *cis*,*cis*-1,3,5-cyclohexanetriol, H_3cht, and 1,1,1-tris(hydroxymethyl)toluene, H_3thmt.

arrays may lead to molecules with large spin ground states. If these arrays consists of simple [M_3] equilateral triangles then the resultant competing exchange interactions or 'spin frustration' stabilises the non-zero spin ground state. If the arrays consist of [M_4] centred triangles (or 'metal stars') in which the three peripheral ions are connected only to the central ion and not to each other, then the antiferromagnetic interaction between these ions stabilises the large spin state. If these 'high spin' triangular units can then be linked together into elaborate polymetallic arrays then the resultant complexes could well be characterised by large spin ground states. In polyoxometallate chemistry[18] it was shown that the disposition of the three alkoxide arms of the *tri-anion* directs the formation of triangular [M_3] units where each arm of the ligand bridges one edge of the triangle. These units then combine to form complexes whose structures are commonly based on octahedra. For clusters of 3d metals however, these units can combine in more diverse ways and produce more elaborate products whose structures are dependent on both (a) the level of deprotonation of the ligand *i.e.* tripod^{3-}, Htripod^{2-} or H_2tripod^{1-} and (b) the presence of other bridging and/or terminal co-ligands such as carboxylates or β-diketonates *etc*.

Manganese clusters

In order to make clusters containing Mn^{III} and/or Mn^{IV} ions it is generally necessary to either oxidise simple Mn^{II} salts, reduce Mn^{VII} salts or use preformed metal clusters such as the oxo-centred triangles $[Mn_3O(O_2CR)L_3]^{0/+}$ (R = Me, Ph *etc*., L = py, MeCN *etc*.).[9]

Reaction of H_3thme with the neutral triangle $[Mn_3O(O_2CMe)_6(py)_3]$ in MeCN leads to the formation of the nonanuclear species $[Mn_9O_7(O_2CMe)_{11}(thme)(py)_3(H_2O)_2]$ (**1**, Fig. 1).[20] The metallic skeleton of **1** comprises a series of ten-edge-sharing triangles that describes part of an idealised icosahedron in which three of the twelve vertices are missing. The $[Mn^{IV}{}_3Mn^{III}{}_4Mn^{II}{}_2O_7]^{14+}$ central core can be described as either a series of vertex- and edge-sharing $[Mn_3O]$ units, or perhaps most easily as a $[Mn^{III}{}_4Mn^{II}{}_2O_6]^{4+}$ ring on which is sitting a smaller $[Mn^{IV}{}_3O]^{10+}$ ring. Antiferromagnetic interactions between the ferromagnetically coupled Mn^{IV} ions in the $[Mn^{IV}{}_3O]^{10+}$ ring and the Mn^{III} and Mn^{II} ions in the $[Mn^{III}{}_4Mn^{II}{}_2O_6]^{4+}$ ring lead to the stabilisation of an $S = 17/2$ spin ground state. This is analogous to the situation in $[Mn_{12}O_{12}(O_2CR)_{16}(H_2O)_4]$ where the four ferromagnetically coupled Mn^{IV} ions couple antiferromagnetically with the surrounding eight Mn^{III} ions.[1] Magnetisation data, collected in the 0–70 kG and 1.8–4.0 K ranges, were fitted by a matrix-diagonalisation method to a model that assumes only the ground state is populated, includes axial zero-field splitting ($D\hat{S}_z{}^2$), and carries out a full powder average—the corresponding Hamiltonian is given in eqn (1).

$$\mathcal{H} = D\hat{S}_z{}^2 + g\mu_B\mu_0\hat{S}_zH_z \qquad (1)$$

The best fit parameters were: $S = 17/2$, $g = 1.97(3)$ and $D = -0.29$ cm^{-1}. Frequency-dependent out-of-phase ac susceptibility signals observed at $T \leqslant 4$ K were fitted to the Arrhenius equation to give an effective energy barrier for the reorientation of the magnetisation (U_{eff}) of 27 K, with $\tau_0 = 5.0 \times 10^{-8}$ s. Single-molecule magnetism behaviour was confirmed by the presence of temperature and sweep rate dependent hysteresis loops in single crystal *M vs. H* studies (Fig. 1) performed on an array of micro-SQUIDs.[21] The loops are not smooth, showing steps at regular intervals of field indicative of quantum tunnelling of the magnetisation (QTM). Inelastic Neutron Scattering (INS) studies on complex **1** confirm the $S = 17/2$ ground state and analysis of the INS transitions within the zero-field split ground state lead to determination of the axial anisotropy, $D = -0.249$ cm^{-1} and the crystal field parameter, $B_4^0 = 7(4) \times 10^{-6}$ cm^{-1}. Frequency domain magnetic resonance spectroscopy

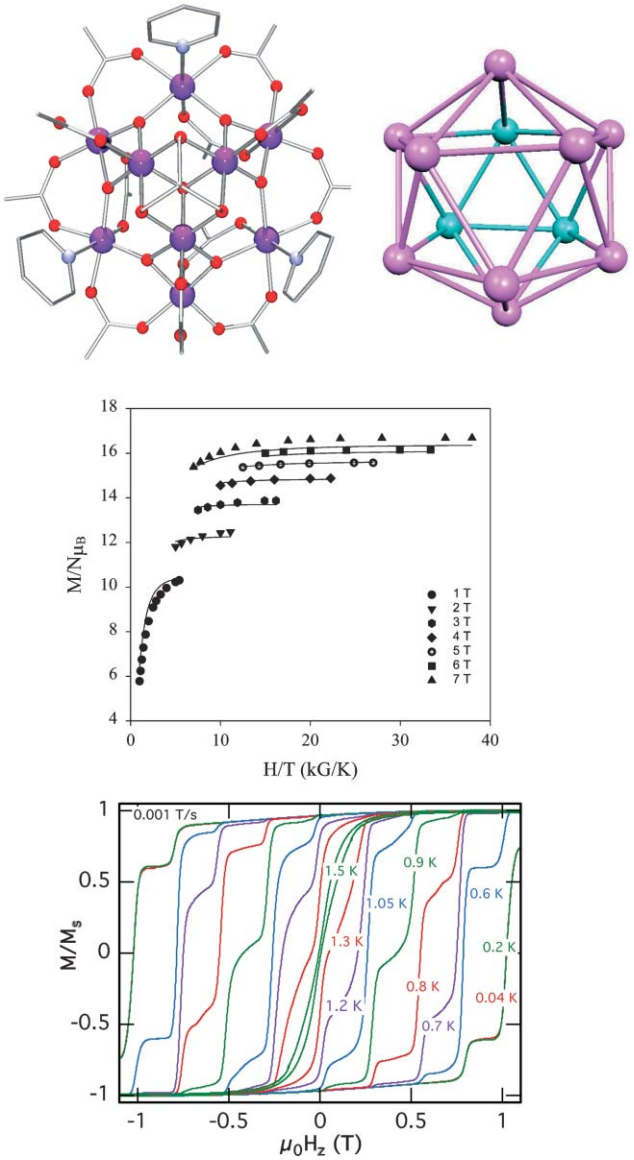

Fig. 1 The structure of complex **1** (top left; colour scheme, Mn = pink, O = red, N = blue, C = grey). Idealised icosahedron (top right), the light blue atoms represent the missing vertices. Reduced magnetisation *vs. H*/*T* for complex **1** (middle). Single crystal magnetisation (*M*) of **1** *vs*. applied magnetic field (*H*) (bottom), the magnetisation is normalised to its saturation value. The resulting hysteresis loops are shown at different temperatures at the indicated field sweep rate.

(FDMRS) determined the same parameters to be $D = -0.247\ cm^{-1}$ and $B_4^0 = +4.6 \times 10^{-6}\ cm^{-1}$.[20] DFT calculations are also fully consistent with the experimental findings of two Mn^{II} and four Mn^{III} ions 'spin up' and three Mn^{IV} ions 'spin down' resulting in the $S = 17/2$ spin ground state of the molecule, with $D = -0.23\ cm^{-1}$ and $U = 26.2$ K.[20]

Repeating the reaction that produced **1** but simply changing the carboxylate from $MeCO_2^-$ to $PhCO_2^-$ produces a completely different product: the dodecanuclear cluster $[Mn_{12}O_4(OH)_2(PhCO_2)_{12}(thme)_4(py)_2]$ (**2**).[22] The core of complex **2** (Fig. 2) consists of a trapped-valence $[Mn^{III}_{10}Mn^{II}_2O_4(OH)_2]^{24+}$ rod- or ladder-like unit consisting of ten edge-sharing $[Mn_3O]$ triangles as directed by the presence of four fully deprotonated $thme^{3-}$ ligands which sit directly above and below the metal 'plane'. The best fit of the magnetisation data gave $S = 7$, $g = 1.98$ and $D = -0.13$ K. This *intermediate* value of S presumably arises because of the numerous triangular metal–metal interactions present and the resultant competing exchange interactions of comparable magnitude that prevent the spin alignments that would normally be preferred. Single crystal studies again reveal the presence of a hysteresis loop whose coercivity was strongly temperature and time dependent, increasing with decreasing temperature and increasing field sweep rate, as expected for the superparamagnetic-like behaviour of an SMM with a blocking temperature (T_B) of $\sim$1.3 K.[22] Above this temperature no hysteresis is observed since the spin relaxes to equilibrium faster than the timescale of the hysteresis loop measurement. Relaxation data determined from dc relaxation decay measurements show that above approximately 0.3 K the relaxation rate is temperature dependent and a fit to the Arrhenius law yielded $\tau_0 = 1.6 \times 10^{-7}$ s and $U_{eff} = 18.3$ K. Below *ca.* 0.3 K however, the relaxation rate is temperature-independent with a relaxation rate of 3×10^7 s indicative of QTM between the lowest energy $Ms = \pm 7$ levels of the ground state.

Again repeating the reaction that gave complex **1**, but this time changing the carboxylate to $Me_3CCO_2^-$ produces the complex $[Mn_8O_4(Me_3CCO_2)_{10}(thme)_2(py)_2]$ (**3**), whose structure is remarkably similar to that of complex **2** (Fig. 2).[22] This time however the core consists of a smaller $[Mn^{III}_8O_4]^{16+}$ rod- or ladder-like unit consisting of six edge-sharing triangles, but again the $thme^{3-}$ ligands are fully deprotonated and sit above and below the plane of the central six Mn^{III} ions. Magnetisation data collected in the ranges 1.8–10 K and 0.10–4.0 T gave a best fit of $S = 6$, $g = 1.81$ and $D = -0.36$ K. However, despite the magnitude of S and sign of D, no out-of-phase ac susceptibility signals were observed indicating that complex **3** is not an SMM. Single crystal micro-SQUID studies at low temperatures indicate the presence of intermolecular interactions—the result is the observation of S-shaped curves with no temperature or sweep rate dependence indicating that the intermolecular interactions are actually relatively strong, consistent with the presence of the bulky pivalate ligands and the packing of the molecules in the crystal. These interactions are antiferromagnetic and thus the result is the destruction of any potential SMM behaviour that the *isolated* individual clusters may have shown. This is actually a rather common occurrence and a good reminder of the importance of

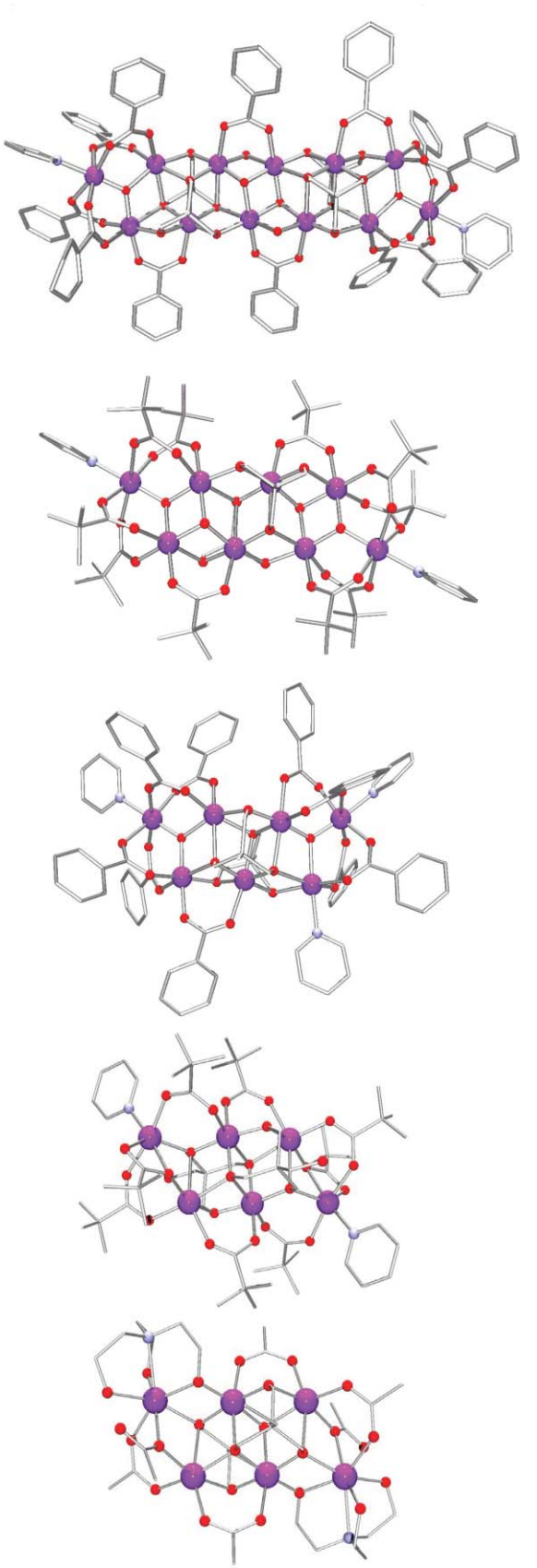

Fig. 2 The structures of the five related 'manganese rods': complexes **2** (top)–**6** (bottom).

considering intermolecular interactions when understanding and explaining the observed physical properties.

Repeating the reaction that produces complex **2**, but in the presence of pyridine, affords the related heptanuclear complex $[Mn_7O_2(PhCO_2)_9(thme)_2(py)_3]$ (**4**).[22] The structure (Fig. 2) closely resembles complexes **2** and **3** with a core containing a trapped-valence $[Mn^{III}{}_5Mn^{II}{}_2O_2]^{15+}$ rod- or ladder-like unit consisting of five edge-sharing triangles. Indeed complex **2** can be regarded as two fused $[Mn_7]$ molecules. Once again the two tripodal ligands are fully deprotonated sitting above and below the plane of the central Mn ions. This complex exhibits a spin ground state of $S = 7$ with $D = -0.20$ K, but like complex **3** shows no sign of SMM behaviour because of significant intermolecular interactions.

A number of related hexanuclear 'rods' have also been isolated and these can all be placed in two categories, exemplified by the complexes $[Mn_6(Me_3CCO_2)_8(tmp)_2(py)_2]$ (**5**) and $[Mn_6(MeCO_2)_6(tmp)_2(H_2tea)_2]$ (**6**, H_3tea = triethanolamine).[22] Both complexes (Fig. 2) contain similar $[Mn^{III}{}_2Mn^{II}{}_4]^{14+}$ rod- or ladder-like units consisting of four edge-sharing triangles with the central two Mn ions being the sole Mn^{III} ions.

The major difference between the two complexes comes in the ligation of the outermost Mn^{II} ions. In complex **5** and its analogues the peripheral ions are connected to the central ions *via* a combination of tripodal ligands and carboxylates, while in complex **6**, and its analogues, the bridging involves tripodal ligands, carboxylates and triethanolamine ligands, where the triethanolamine ligands simply replace the one pyridine molecule and one μ,η^1,η^2 carboxylate present in **5**. In complex **6** all six Mn ions lie in the same plane, while in complex **5** the two outermost Mn ions lie above and below the plane of the four central Mn ions changing the bridging angles of the μ_3-oxygen arm of the tripodal ligand that links the peripheral Mn^{II} ions to the central Mn^{III} ion. The result is a much larger distortion to the metal–oxygen core in complex **5** and this has important consequences for the observed magnetic properties of the two species, which differ considerably despite the obvious similarity between the metal topologies.[22] Unfortunately the presence of multiple Mn^{II} ions means that no satisfactory fit of the magnetisation data could be obtained for either complex. Mn^{II} ions promote weak exchange interactions, the result of which is the presence of a large number of S states with comparable energies to the ground state. It is also impossible to determine the individual pairwise exchange constants J_{ij} between Mn_iMn_j pairs through conventional methods as, for both **5** and **6**, there are five chemically different exchange interactions. However the problem can be addressed through the use of density functional calculations. DFT calculations of the magnetic exchange between paramagnetic metal ions is a new and appealing approach to understanding the magnetic behaviour of 'large', complicated paramagnetic clusters.[8] Here calculations yield a spin ground state of $S = 4$ for **5** and $S = 0$ for **6**, with all the interactions being weakly ferromagnetic or weakly antiferromagnetic (**5**: $J_1 = -5.99$, $J_2 = -0.72$, $J_3 = +3.02$, $J_4 = +0.31$, $J_5 = +1.46$ cm^{-1}; **6**: $J_1 = +2.44$, $J_2 = +0.08$, $J_3 = +0.98$, $J_4 = -2.00$, $J_5 = -0.39$ cm^{-1}). The obtained ground state spin structures for both are summarized in Fig. 3.[22]

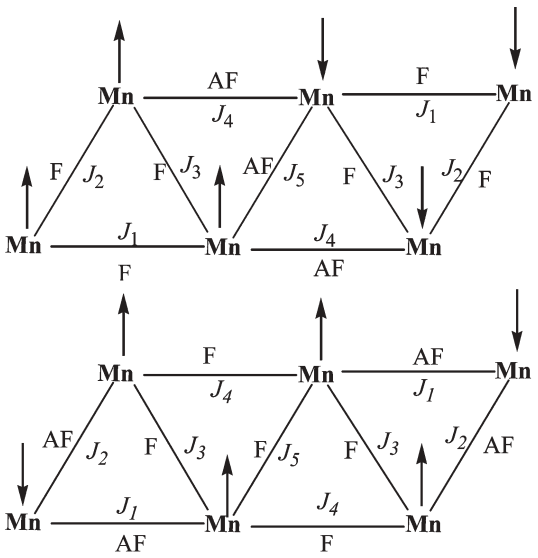

Fig. 3 Ground state spin structures of **5** and **6**. F = ferromagnetic, AF = antiferromagnetic. 'Spin-up' and 'spin-down' has been assigned based on the sign of the exchange interactions obtained using DFT.

The syntheses and structures of these rod-like complexes (**2–6**) are an excellent example of how even small changes in reaction conditions can be used to generate a family of related compounds. Although the actual mechanisms for the formation of these species are likely to be extremely complicated, involving the protonation/deprotonation, oxidation/reduction and structural rearrangement of several species in solution, the presence of deprotonated (tripod^{3-}) tripodal ligands will always favour the isolation of clusters based on shared $[M_3]$ units. Of course this may not be the case where the tripod is only partly deprotonated (Htripod^{2-} or H_2tripod^{1-}) or where there are more drastic changes in reaction conditions, like, for example, a change in solvent.

The use of alcohol in the synthesis of Mn SMMs had, until recently,[9,23] generally been avoided when using preformed Mn clusters (like the oxo-centred metal triangles above) as starting materials, since it would inevitably lead to the reduction of the Mn centres and the protonation of the oxo- and/or hydroxo groups that are *generally* responsible for holding these large Mn aggregates together. However recently it has been shown that alcohol induced structural rearrangement and 'reductive aggregation' are elegant synthetic strategies.[24] Reaction of the triangle $[Mn_3O(O_2CMe)_3(HIm)_3]O_2CMe$ with H_3tmp in MeOH does not produce a rod-like species as it does in MeCN, but instead affords the wheel-like complex $[Mn_{22}O_6(OMe)_{14}(O_2CMe)_{16}(tmp)_8(HIm)_2]$ (**7**, Fig. 4).[25] This is a mixed-valent $[Mn^{IV}{}_2Mn^{III}{}_{18}Mn^{II}{}_2]$ complex comprising a series of linked $[Mn_3O]$ triangles and partial $[Mn_4]$ cubanes—similar to that seen in the largest known SMM, $[Mn_{84}]$.[24] Complex **7** has a spin ground state of $S = 10$ with $D = -0.10$ cm^{-1} and is a rare example of a cyclic, high-spin Mn SMM. The hysteresis loops (Fig. 4) do not show the step-like features indicative of quantum tunnelling of magnetisation between the energy states of the molecule. This absence can be rationalised as primarily due to a distribution of molecular environments (a common feature of larger clusters and/or those displaying a degree of

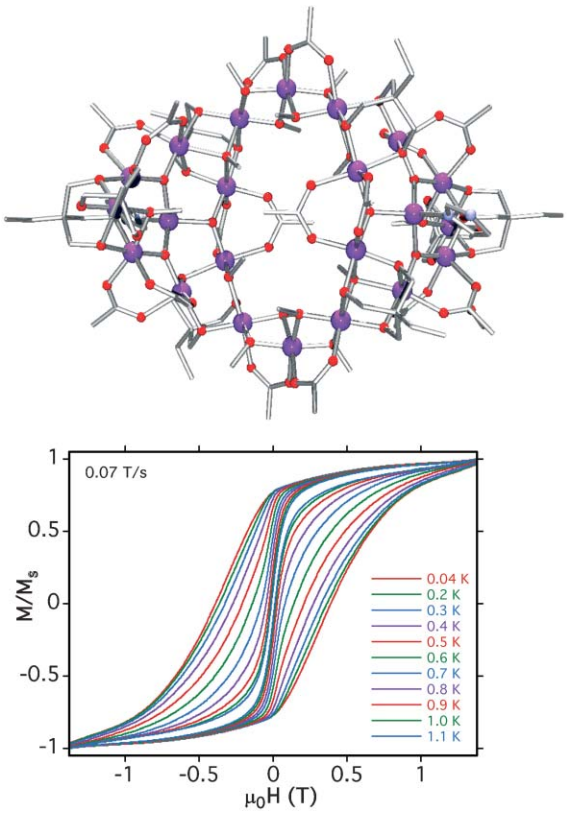

Fig. 4 The structure of complex **7** (top); magnetisation (*M*) *vs.* dc field (*H*) hysteresis loops for **7** at a field scan rate of 0.07 T s^{-1} in the temperature range 1.1 - 0.04 K (bottom).

disorder) and thus a distribution of magnetisation relaxation barriers. In addition, weak intermolecular interactions (exchange and/or dipolar) and low-lying excited states will also contribute to the broadening of steps. Relaxation measurements between 0.04 and 1.2 K yield the values $\tau_0 = 3 \times 10^{-11}$ s and $U_{eff} = 19$ K. Below approximately 0.3 K the relaxation rate becomes temperature-independent suggesting the presence of QTM.

Aside from the well used [Mn_3] 'triangles' another useful starting material is the dinuclear complex [$Mn_2O_2(bpy)_4$](ClO_4)$_3$.[26] This complex contains high oxidation state Mn ions ([$Mn^{IV}Mn^{III}$]) and is easy to make in large quantities and it is thus an ideal starting material. In fact there exist many such small high oxidation state Mn compounds in the literature that, as yet, are untried candidates for use in Mn cluster synthesis. Reaction of [$Mn_2O_2(bpy)_4$](ClO_4)$_3$ with H_3thme or H_3tmp in MeCN produces the dimetallic complexes [Mn_2(Htripod))$_2$(bpy)$_4$](ClO_4)$_2$ (**8**, Htripod = Hthme; **9**, Htripod = Htmp; Fig. 5).[27] Here the partial deprotonation of the ligands is accompanied by a reduction of one of the Mn ions. The two Mn^{III} ions couple ferromagnetically through the alkoxide bridges to give a ground state of $S = 4$, with $D = -0.65$ cm^{-1}, but the analysis of the magnetism is hindered by the weak exchange and resultant low-lying excited states. Single crystal micro-SQUID measurements do however show the existence of temperature and sweep rate dependent hysteresis loops at low temperature, suggesting complex **8** to be only the second example of a dinuclear Mn SMM after the

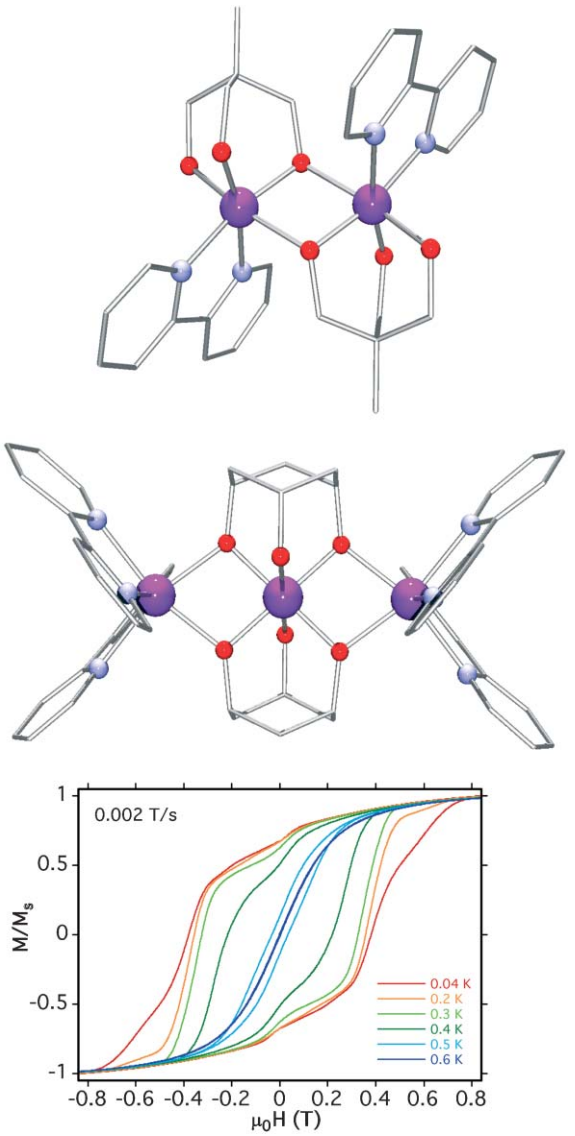

Fig. 5 The structures of complexes **8** (top) and **10** (middle). Magnetisation (*M*) *vs.* dc field (*H*) hysteresis loops for **10** (bottom).

complex [Mn_2(saltmen)$_2$(ReO_4)$_2$].[28] Replacing H_3thme or H_3tmp with another tripodal ligand, H_3cht, in the same reaction scheme produces the trinuclear SMM [$Mn^{III}Mn^{II}_2$-(Hcht)$_2$(bpy)$_4$](ClO_4)$_2$ (**10**, Fig. 5).[29] Again the aggregation process is accompanied by reduction of the Mn ions and partial deprotonation of the ligand. The complex consists of a linear trinuclear array of Mn ions linked by alkoxide oxygens where the central metal is the sole Mn^{III} ion. Magnetic studies show the metal centres to be ferromagnetically coupled to give a ground state of $S = 7$, with $D = -0.10$ cm^{-1}. Single crystal *M vs. H* measurements reveal the presence of a hysteresis loop whose coercivity was strongly temperature and time dependent (Fig. 5) with a blocking temperature of $\sim$0.5 K. Complex **10** is the only trinuclear homometallic SMM reported to date and the first Mn SMM to contain only one Mn^{III} ion.

Because complexes **8** and **9** can be made in high yield they themselves have also served as extremely useful starting materials for the synthesis of much larger complexes. For

example, reaction of complex **8** with NaN_3 and NaO_2CMe in MeCN leads to the isolation of the cluster $\{Mn(bpy)_3\}_{1.5}$-$[Mn_{32}(thme)_{16}(bpy)_{24}(N_3)_{12}(OAc)_{12}](ClO_4)_{11}$ (**11**, Fig. 6).[30] The $[Mn_{32}]^{8+}$ cation consists of eight $[Mn^{IV}{}_1Mn^{II}{}_3]$ centred-triangles (or 'metal stars') linked together to form a truncated cube with each $[Mn_4(thme)_2]^{4+}$ corner unit linked to its nearest neighbours along each edge *via* $CH_3CO_2^-$ and N_3^- ligands.

Unfortunately the magnetic properties of the compound are complicated by both the presence of the multiple Mn^{II} ions and ligand counter-complementarity. Magnetic susceptibility measurements on complex **11** are indicative of dominant antiferromagnetic exchange between the metal centres with the $\chi_M T$ value at 2 K in the region expected for an $S = 9$ or 10 ground state. Ac measurements (which avoid Zeeman and other effects of an applied dc field)[31] taken in the temperature range 10–1.8 K show steeply sloping lines with a rapid decrease in $\chi'_M T$ with decreasing temperature suggesting the population of many excited states with larger S values. This is a common feature in many Mn clusters that are either (a) of high nuclearity and thus possess a large density of spin states; or (b) contain multiple Mn^{II} ions. Extrapolation of the $\chi'_M T$ signal from values above $\sim$3 K (to avoid decreases due to such effects as intermolecular interactions at lower temperatures) to 0 K gives a value consistent with the dc data and suggests a spin ground state of $S = 9$ or 10. Magnetisation measurements also confirm the presence of many excited states. Studies on a single crystal at temperatures down to 40 mK and in fields up to 1.2 T performed on a micro-SQUID set-up show curves that do not reach saturation. For all temperatures studied, the magnetisation rises sharply with increasing field strength. This is as expected for field-induced stabilisation of *Ms* levels of excited states with S values greater than that of the ground state; approach to, and crossing of excited state *Ms* levels with those of the ground state leads to increases in the measured magnetisation. Thus, for example, the magnitude of the magnetisation at 40 mK in an applied field of 1 T is suggestive of $S \geqslant 25$. Similarly, magnetisation measurements carried out on a powdered crystalline sample in temperatures below 10 K in fields up to 7 T saturate at a value of $M/N\mu_B \approx 85$, consistent with the stabilisation of an $S \geqslant 43$ spin state (with $g = 2.0$). However when smaller applied fields are used the magnitude of $M/N\mu_B$ decreases and does not saturate. Application of strong magnetic fields effectively overcomes weak antiferromagnetic exchange, stabilising spin states with larger values of S. If we were to assume the interaction between the central Mn^{IV} ion and the three peripheral Mn^{II} ions within an isolated $[Mn^{IV}Mn^{II}{}_3]$ unit to be antiferromagnetic, then we would expect a spin ground state of $S = 6$ for this unit. Between each of these corner units the *syn*,*syn* μ-$CH_3CO_2^-$ ligands are likely to promote antiferromagnetic exchange, but the end-on N_3^- ligands, ferromagnetic exchange. If the antiferromagnetic interactions were to dominate then we might expect to observe an overall spin ground state of $S = 0$, but if the ferromagnetic interactions were to dominate then an $S = 48$ ground state may result. However, there are a total of twenty-four Mn^{II} ions present in the $[Mn_{32}]^{8+}$ cation, the result of which is likely to be a large number of S states with comparable energies to the ground state. This 'problem' is then further compounded by the fact the $[Mn^{IV}Mn^{II}{}_3]$ units are linked together by two different ligands—one azide and one carboxylate—and this counter-complementarity will likely lead to an interaction that is either weakly ferro- or weakly antiferromagnetic, but in either case, near 0 cm^{-1}. Weak intermolecular interactions—if comparable in magnitude to the intracluster exchange—will also complicate the analysis.

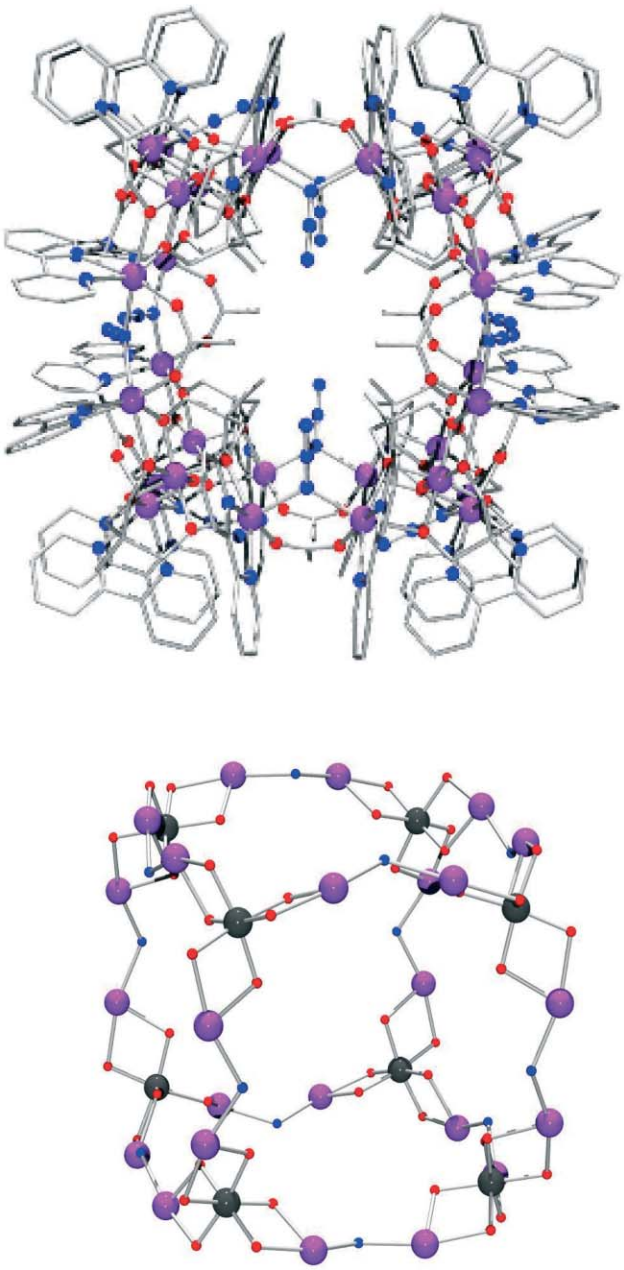

Fig. 6 The structure of complex **11** (top) and its core (bottom). In the lower picture the four corner Mn ions of an 'ideal' cube are highlighted in black.

Iron clusters

The simple reaction between $FeCl_3$ and H_3thme in alcohol produces the tetranuclear clusters $[Fe_4(thme)_2(ROH)_6Cl_6]$ (**12**, R = C_3H_7OH, Fig. 7).[32] The structure describes a centred $[Fe_4]$

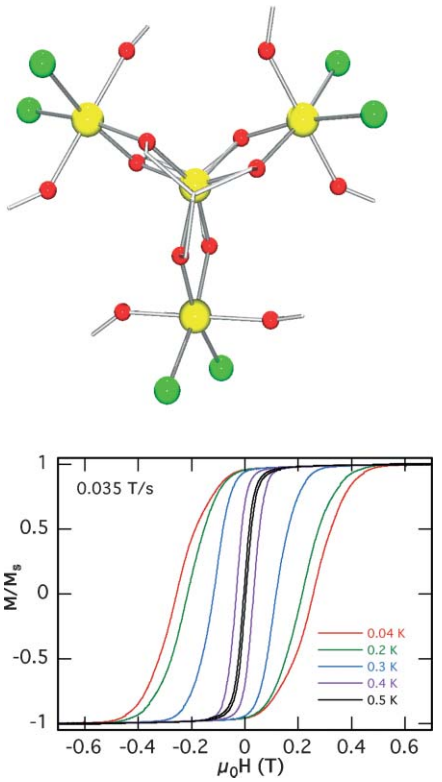

Fig. 7 The structure of complex **12** (Fe = yellow, O = red; Cl = green) (top). Variable temperature hysteresis loops for **12** measured at a field sweep rate of 0.035 T s^{-1} and the indicated temperatures (bottom).

triangle (or 'metal star') consisting of a central Fe^{III} ion connected to three peripheral Fe^{III} ions through two fully deprotonated $thme^{3-}$ ligands that occupy the apical positions of the $[Fe_4]$ skeleton. A similar complex, but containing methoxides and β-diketonates had previously been reported.[33] A ground state $S = 5$ results from the antiferromagnetic coupling between the central and the peripheral iron ions. The experimental data in the range 2–300 K were fitted to the theoretical expression corresponding to the spin Hamiltonian (2):

$$\mathcal{H} = -JS_{Fe1}\cdot(S_{Fe2} + S_{Fe3} + S_{Fe4}) + g\beta H\cdot S \qquad (2)$$

where J corresponds to the exchange coupling parameter between the central Fe ion and the three peripheral Fe ions. The fit of the experimental data gave $J = -28.2$ cm^{-1} with $g = 1.97$ corresponding to a spin ground state $S = 5$ separated by 70.5 cm^{-1} from the first $S = 4$ excited state. A fit of the magnetisation data considering only population of the ground state (and neglecting any intermolecular interactions) gave $S = 5$, $D = -0.32$ cm^{-1}, $E = 0$ and $g = 1.98$. The sign and magnitude of D were confirmed by Q-band EPR spectroscopy performed in the field range 0–1.7 T at $T = 5$ K.[32] The fit of the EPR data gave $D = -0.33$ cm^{-1} and $E = 0.006$ cm^{-1} with $g = 2.03$. Magnetisation measurements performed on a single crystal coupled to a micro-SQUID loop showed hysteresis loops below 1 K with coercivities increasing upon decreasing temperatures and increasing field sweep rates (Fig. 7). No clear steplike features indicative of quantum tunnelling of the magnetisation are present, however, as these are smeared out due to a combination of the disorder associated with the terminal alcohol ligands and the presence of weak ferromagnetic intermolecular interactions.[32]

Introduction of carboxylates into the reaction scheme leads to the isolation of the related clusters $[Fe_9O_4(O_2CCMe_3)_{13}(thme)_2]$ (**13**, Fig. 8) and $[NEt_4][Fe_{11}O_4(O_2CPh)_{10}(thme)_4(dmhp)_2Cl_4]$ (**14**, Fig. 8).[34] Complex **13** has a near planar rhomb or diamond-like array of nine Fe^{III} ions formed from eight edge-sharing $[Fe_3]$ triangles whilst complex **14** comprises ten such $[Fe_3]$ triangles. Despite their structural similarity the two complexes display markedly different magnetic properties. While **13** displays the behaviour expected for a complex exhibiting a $S = 1/2$ spin ground state, complex **14** proved to be much more interesting. The fit of the magnetisation data, made simultaneously on four different temperatures (2, 3, 4 and 6 K) in the field range 0.1–5.5 T, yielded the parameters $S = 11/2$, $g = 2.03$ and $D = -0.46$ cm^{-1}. Its polycrystalline EPR spectrum at Q-band frequency and 5 K confirmed both the spin state and magnitude and sign of the zero-field splitting, though significantly, it was impossible to produce an adequate simulation of the spectrum without inclusion of rhombicity ($E = 0.055$ cm^{-1}). Low-temperature (1.2–0.04 K) single crystal magnetic measurements showed the presence of hysteresis loops in magnetisation *vs.* field studies whose coercivities increase with decreasing temperature. A detailed study of the field sweep rate dependence of the hysteresis loops

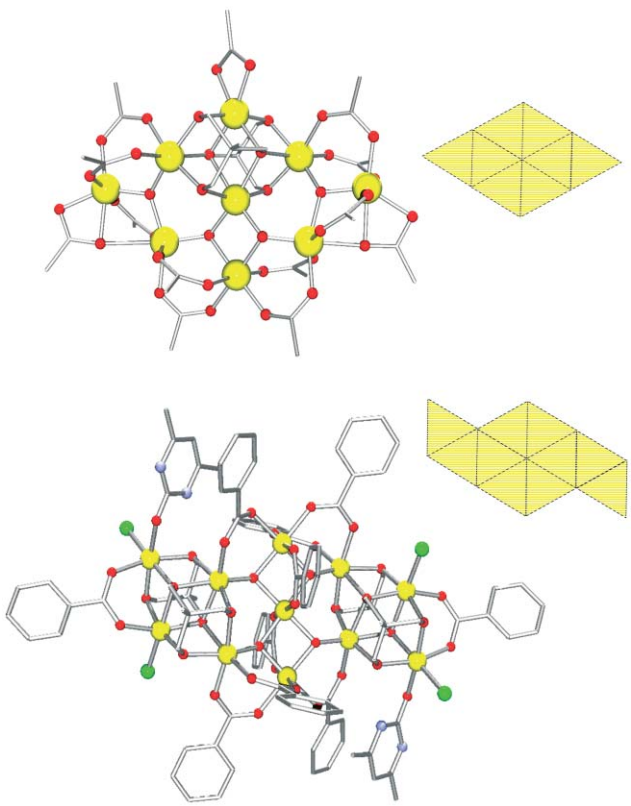

Fig. 8 The structures of complexes **13** (top) and **14** (bottom) and cartoon representations of their metal topologies.

showed that the hysteresis at non-zero fields is not due to a phonon bottleneck but due to slow relaxation because of the anisotropy barrier. Slow relaxation is seen at $H = 0$ but the presence of strong tunnelling does not allow for a reliable Arrhenius plot. For all SMMs the barrier is reduced at $H = 0$ because of the presence of tunnelling. Even for half-integer spin systems which in theory should not tunnel do so because of coupling with the environment: dipolar coupling between molecules, hyperfine coupling, spin–spin cross relaxation, and other multibody quantum processes. For example for a system with $S = 11/2$, $D = -0.46\ cm^{-1}$ and $E = -0.055\ cm^{-1}$, and assuming an internal transverse field of approximately 10 mT, one can estimate a tunnel splitting of *ca.* 2.8×10^{-6} K and thus a tunnel probability of $P = 0.68$ for a sweep rate of $0.1\ Ts^{-1}$.

To date most cluster synthesis has involved 'conventional' coordination chemistry techniques, *i.e.* solution chemistry under atmospheric pressure and at temperatures limited to the boiling points of common solvents. This is largely due to the simple fact that reactions performed under ambient conditions work very well, and there is therefore no perceived need for higher temperatures or pressures. But the application of different temperatures and pressures is likely to lead to the isolation of different products and is therefore an attractive alternative synthetic strategy that should not be ignored. Solvothermal techniques[35] allow the application of high temperatures to reactions in low boiling solvents and are an excellent method for the preparation of pure, crystalline products in high yields. For example, reacting $[Fe_3O(O_2CR)_6(H_2O)_3]X$ (R = Ph, CMe_3; X = NO_3, Cl) with H_3thme in MeCN in a sealed Teflon container at 150 °C for a period of 12 hours produces the octanuclear wheels $[Fe_8(O_2CR)_{12}(thme)_4]$ (**15**, R = Ph; **16**, R = CMe_3; Fig. 9).[36] The tripodal ligands are fully deprotonated but in this instance, and rather unexpectedly, they do not direct the formation of triangular metal units but instead each bridge four iron centres in a semi-circular array. The size of the wheel seen in complex **15** can then be doubled by the addition of a coordinating alcohol in the crystallisation step—use of EtOH, for example, produces the hexadecametallic *square-wheel* $[Fe_{16}(EtO)_4(O_2CPh)_{16}(Hthme)_{12}](NO_3)_4$ (**17**, Fig. 9).[36] The added alcohol protonates one arm of each tripod, the result being that each $Hthme^{2-}$ ligand now forms a near linear array of three metal ions with an ethoxide at each corner of the 'square'. Both wheels are non-planar and perhaps best described as bowl or ladle-shaped with approximate diameters of 8 and 16 Å respectively. As with all even-membered Fe^{III} wheels antiferromagnetic interactions between nearest neighbours results in $S = 0$ spin ground states for both complexes. Both **15** and **17** can be broken down into simple units of two metal ions and the bridging ligands that connect them (Fig. 9). In order to analyse the magnetic behaviour of **15** and **17** exact analytical equations for the χT product as a function of the temperature, using the interaction topologies shown, were found.[36] The best fits of the χ *vs.* T curves in the 300–10 K temperature range were obtained with the following parameters: $g = 2.0$, $J_1 = -22.2\ cm^{-1}$ and $J_2 = -8.5\ cm^{-1}$ for **15**; and $g = 2.0$, $J_1 = -16.0\ cm^{-1}$, $J_2 = -9.1\ cm^{-1}$ and $J_3 = -74.4\ cm^{-1}$ for **17**.

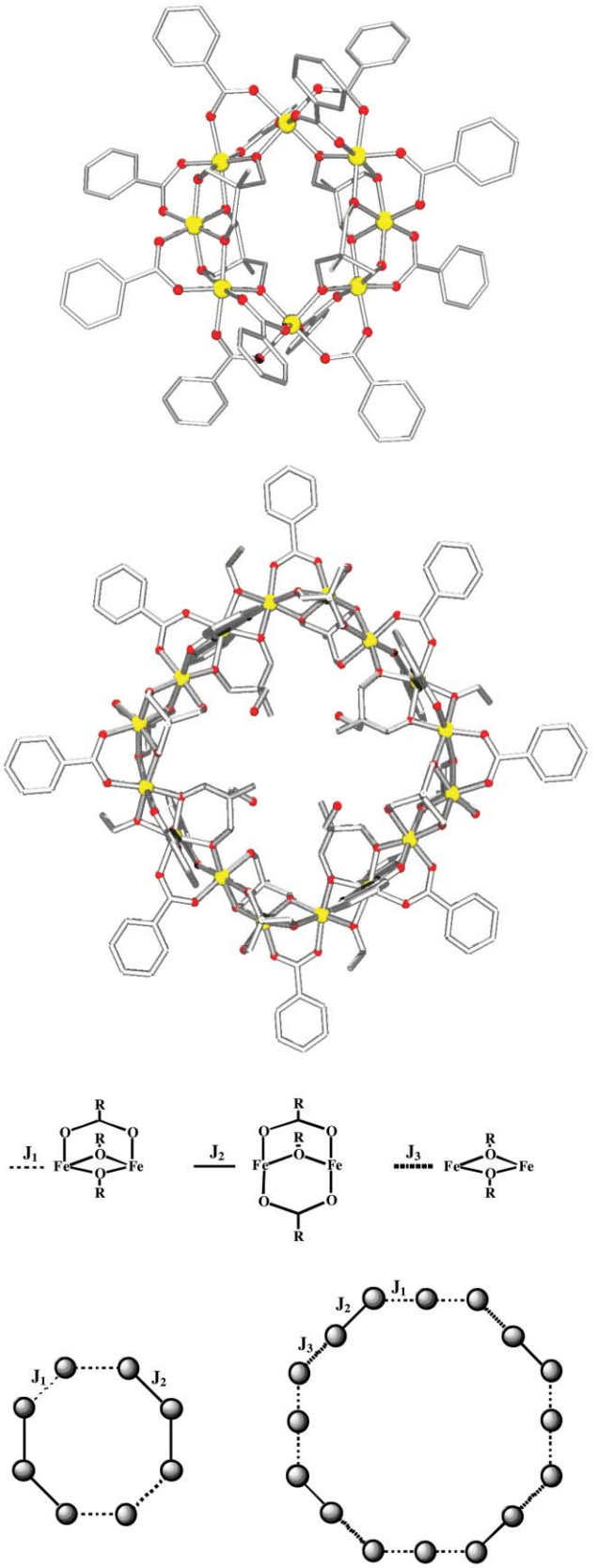

Fig. 9 The structures of complexes **15** (top) and **17** (middle). The dinuclear units (J_1–J_3) used to model the magnetic behaviour and their positions within the wheels (bottom).

Nickel and cobalt clusters

The reaction of $Ni(NO_3)_2$ with H_3thme in the presence of NaOMe leads to a tetranuclear SMM of formula $[Ni_4(H_2thme)_4(CH_3CN)_4](NO_3)_4$ (**18**, Fig. 10) with a cubane-like structure.[37] Intramolecular ferromagnetic interactions ($J = 10$ cm^{-1} based on $\mathcal{H} = -J(S_1.S_2 + S_1.S_3 + S_1.S_4 + S_2.S_3 + S_2.S_4 + S_3.S_4)$) leads to a $S = 4$ ground state stabilised by 40 cm^{-1} from the first $S = 3$ excited state. Magnetisation *vs*. field studies performed at temperatures between 2 and 6 K give best fit parameters of $S = 4$, $D = -0.43$ cm^{-1}, $E/D = 0.04$ and $g = 2.22$. The magnitude of the E parameter is crucial for relaxation *via* quantum tunnelling. For large E/D values one would expect fast relaxation at $H = 0$ because of the relatively large mixing between the $Ms = +4$ and -4 sublevels and this may completely preclude the observation of a hysteresis loop in low temperature magnetisation studies.

For weak rhombicity ($E/D \approx 0$) relaxation *via* quantum tunnelling may still occur, but more slowly, meaning that the hysteresis may well still be present. Micro-SQUID data obtained at temperatures down to 40 mK and at various field sweep rates are shown in Fig. 10. The large step at zero-field occurs when the field is swept from -1 T back to 0 T where the Ms +4 and -4 levels are in resonance and the height of the step indicates that the tunnelling process here is relatively fast. The tunnel probability decreases as the sweep rate is increased and this is manifested in the presence of 'larger' loops. The equivalent cobalt complex $[Co_4(H_2thme)_4(CH_3CN)_4](NO_3)_4$ (**19**, and various analogues such as $[Co_4(H_2thme)_4Br_4]$; **20**, Fig. 10) can be made *via* similar methods by simply replacing $Ni(NO_3)_2$ with $Co(NO_3)_2$ or $CoBr_2$. Again the Co^{II} ions are coupled ferromagnetically and one might therefore expect these complexes to act as SMMs as well. However, magnetisation data measured at temperatures down to 40 mK in fields up to 1 T show no signs of hysteresis (Fig. 10). Indeed despite the large number of Co clusters we have now built with tripodal alcohol ligands[38] *none* have been found to display single-molecule magnetism behaviour.

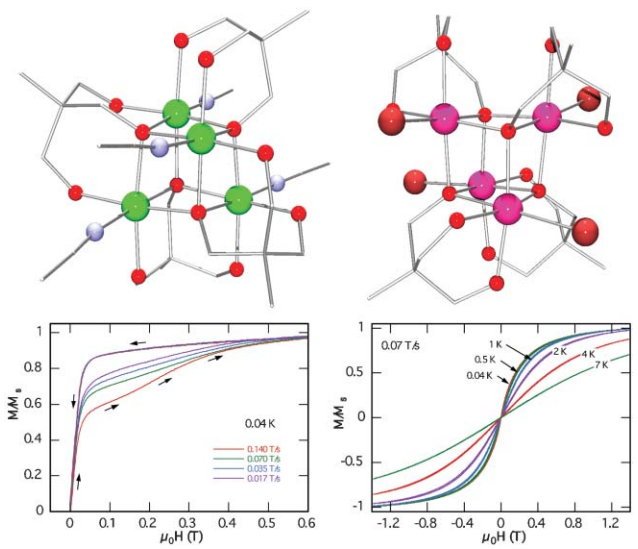

Fig. 10 The structures of **18** (top left) and **20** (top right) and their respective low temperature single crystal M *vs*. H plots. Ni = green; Co = pink; O = red; N = blue; Br = brown.

Thus far we have structurally characterised fewer nickel clusters, but fortunately their magnetic properties have proved more interesting. For example, reaction of $Ni(acac)_2$ with H_3tripod and NaN_3 in alcohol leads to the isolation of the decametallic species $[Ni_{10}(tripod)_2(N_3)_8(acac)_6(MeOH)_6]$ (thme = **21**; tmp = **22**, Fig. 11).[39] These complexes possess a core containing a planar disc-like $[Ni^{II}_{10}O_{10}N_8]^{2+}$ unit held together by a combination of fully deprotonated tripod^{3-} and N_3^{1-} ligands describing a total of ten edge-sharing $[Ni^{II}_3]$ triangles.

It is well known that end-on bridging azide ligands often mediate ferromagnetic exchange between paramagnetic centres and magnetostructural correlations between the strength of the interaction and the M–N–M angle in these bridges have now been reported for both Cu^{II} and Mn^{II}.[40] This property has recently started to be exploited in the preparation of SMMs, elegant examples of which include the synthesis of a $[Fe_9]$ cluster[41] in which μ_4-OH^- ions are deliberately replaced by μ_4-N_3^- ions and in the synthesis of a $[Mn_{25}]$ cluster that possesses a spin ground state of $S = 51/2 \pm 1$.[17] Variable temperature dc magnetic measurements for complex **22** show ferromagnetic exchange between the metal ions resulting in a $S = 10$ spin ground state with appreciable zfs. Frequency-dependent out-of-phase ac susceptibility signals are observed at $T \leqslant 3$ K but no peaks are seen. Single crystal M *vs*. H studies (Fig. 11) performed on a micro-SQUID show temperature and sweep rate dependent hysteresis loops proving **22** to be a new and rather rare example of a ferromagnetic Ni SMM with an effective energy barrier of approximately 14 K for the reorientation of the magnetisation. This is amongst the largest yet seen for any Ni SMM.

The problems we have encountered in isolating crystalline Ni-tripod clusters under ambient conditions, despite much effort, again led us to solvothermal techniques. Reaction of $[Ni(dbm)_2]$ and H_3thme in EtOH at 150 °C in a Teflon-lined autoclave gave the decametallic complex $[Ni_{10}O(thme)_4(dbm)_4(O_2CPh)_2(EtOH)_6]$ (**23**, Fig. 12).[42] The core of **23** is a highly regular $[Ni_{10}]$ super-tetrahedron centred on the sole μ_6-O^{2-} ion. Each of the four triangular $[Ni_6]$ faces is near-planar and they are held together by one fully deprotonated μ_6-thme^{3-} ligand. An alternative view of the core is as four $[Ni_4O_4]$ cubanes each sharing one edge with the other three and all sharing the common oxide vertex (Fig. 12, bottom). In isolated cubanes (like complex **8**) the arrangement with respect to the metal ions is tetrahedral. Fused cubanes give rise to higher nuclearity clusters as exemplified by a tridecametallic Mn super-cubane.[43] Metal octahedra, supertetrahedra and supercubanes are all related: capping alternate faces of an octahedron gives the supertetrahedron and capping the remaining four faces gives the supercubane. As such these species can be considered trapped fragments of a parent mineral lattice. Here each face of **23** corresponds to a {1,1,1} plane of bulk NiO. NiO is an antiferromagnet where the strong interactions across linear Ni–O–Ni ($\sim$180°) units dominates. Ni^{II} cubanes like complex **8** however are generally weakly ferromagnetically coupled *via* approximately right-angled ($\sim$90°) Ni–O–Ni units. For complex **23** the high temperature

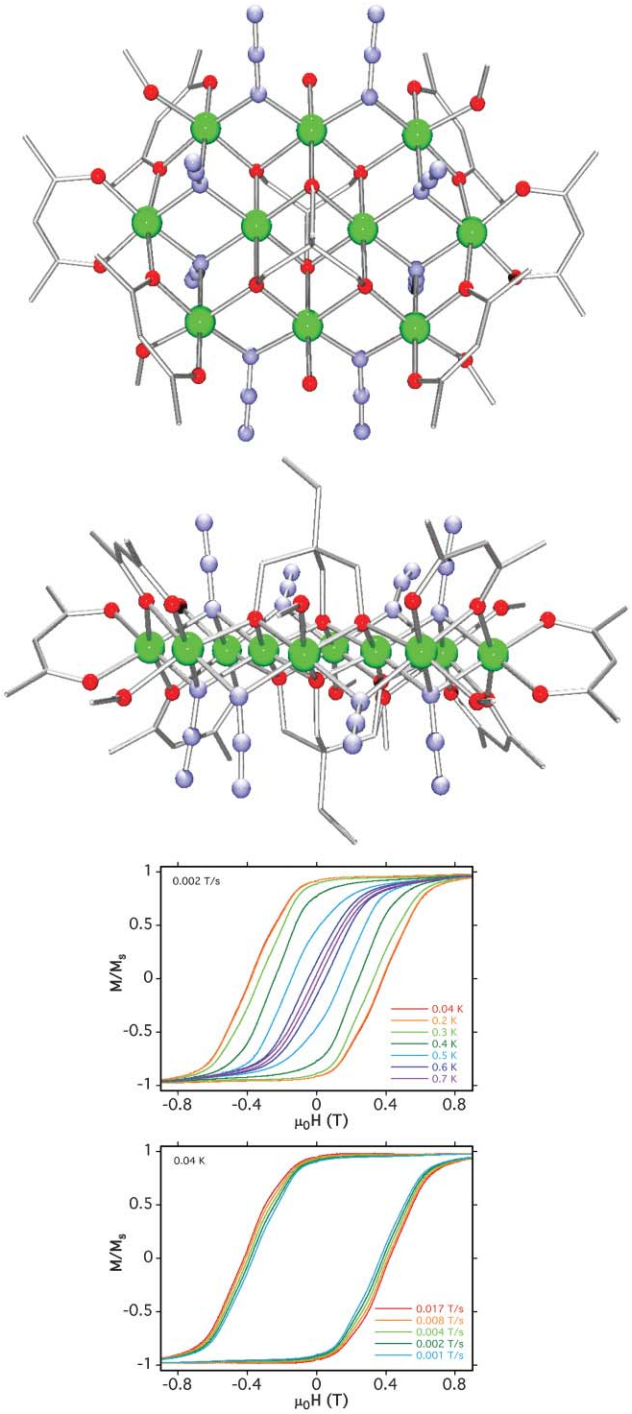

Fig. 11 The structure of complex **22** viewed (a) perpendicular to the $[Ni_{10}]$ plane (top), and (b) parallel to the $[Ni_{10}]$ plane (middle). Magnetisation (*M*) *vs*. applied dc magnetic field (*H*; bottom) at the indicated field sweep rates and temperatures; the magnetisation is normalised to its saturation value.

susceptibility data is in fact dominated by the antiferromagnetic linear moiety (best fit: $J = -62$ cm^{-1}) and is thus analogous to the behaviour of bulk NiO ($J = -70$ cm^{-1}). At low temperature one might expect the properties to be dominated by the coupling of the vertex Ni ions. Although these would be coupled rather weakly the supertetrahedral

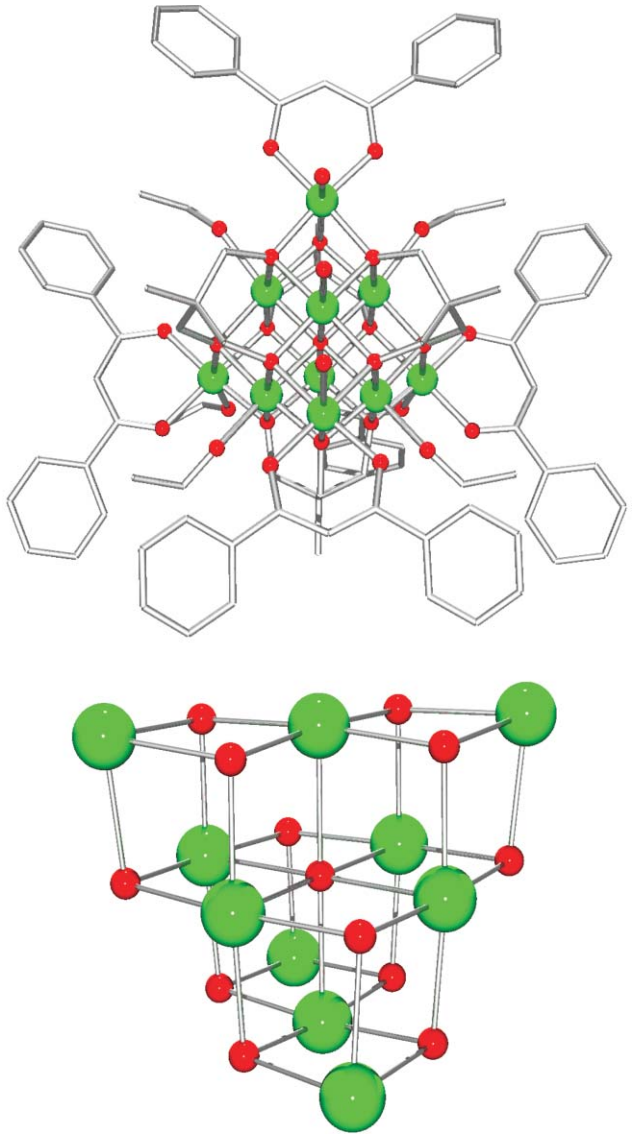

Fig. 12 The structure of complex **23** (top) and its metal-oxygen core (bottom) showing the four fused cubane units.

array would lead to spin frustration with the cluster probably having near-degenerate states with $S = 0$ to $S = 4$. However, below 40 K the $\chi_M T$ product rises sharply with an inverse field dependence, indicative of magnetic ordering consistent with the packing of **23** in the crystal. Zero-field cooled, field cooled and remnant magnetisation data are consistent with this, revealing a non-vanishing net magnetisation.

Ligand bridging modes

The bridging modes displayed by the ligands tripod^{3-}, Htripod^{2-} and H$_2$tripod^{1-} (where tripod = thme, tmp, Hpeol and cht) in complexes **1–23** are shown in Fig. 13. When fully deprotonated (tripod^{3-}) the ligands usually direct the formation of arrays based on edge-sharing metal triangles. These include a 'supertriangle' comprising four edge-sharing triangles (*e.g.* **23**) in which the ligands adopt an $\eta^3,\eta^3,\eta^3,\mu_6$ mode; rod-like pentamers comprising three edge-sharing

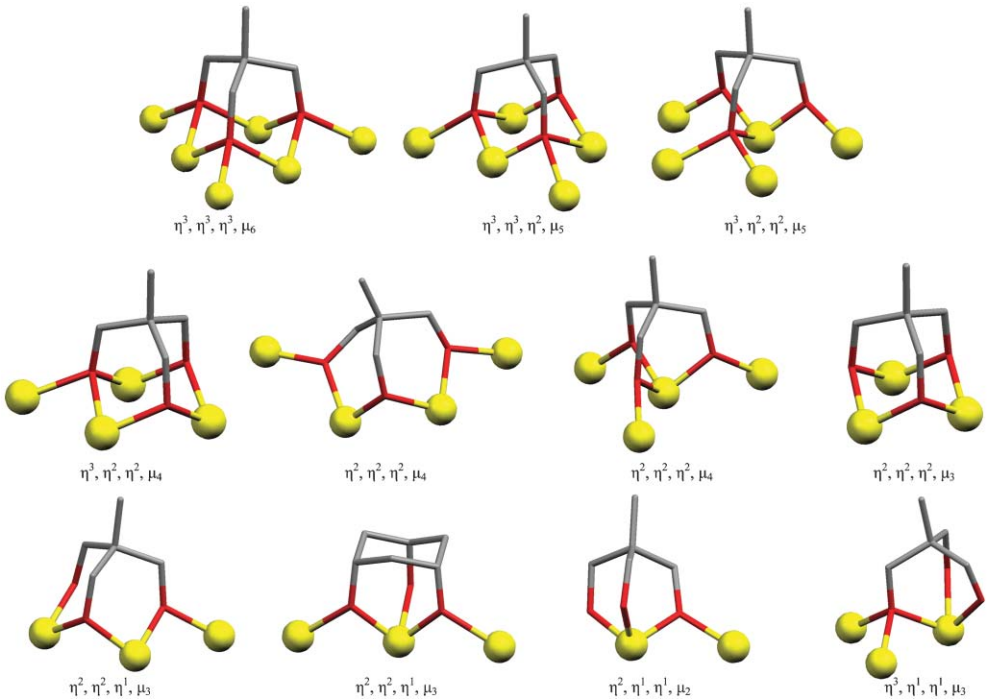

Fig. 13 The bridging modes displayed by the tripodal alcohols tripod^{3-} (top two rows, tripod = thme, tmp, Hpeol and cht), Htripod^{2-} and H$_2$tripod^{1-} (bottom row) in complexes **1–23**. Colour scheme, metal = yellow; oxygen = red; carbon = grey.

triangles (**2–6**) where the ligands adopt either an $\eta^3,\eta^3,\eta^2,\mu_5$ or $\eta^3,\eta^2,\eta^2,\mu_5$ mode; a rhomb comprising two edge-sharing triangles (**14**) in which the ligands adopt an $\eta^3,\eta^2,\eta^2,\mu_4$ mode; a centred [M$_4$] triangle (or 'metal star') (**12**) where the ligands adopt an $\eta^2,\eta^2,\eta^2,\mu_4$ mode; and a simple [M$_3$] triangle (**1**) where the ligands adopt an $\eta^2,\eta^2,\eta^2,\mu_3$ mode. The only exception to this is seen in complex **15**—the octametallic Fe^{III} wheel—where the ligands adopt an $\eta^2,\eta^2,\eta^2,\mu_4$ mode whereby the metal ions are arranged in a semi-circular fashion.

When the tripods are only doubly (Htripod^{2-}) or singly (H$_2$tripod^{1-}) deprotonated the resultant metal–metal arrangement *appears* to favour a more linear topology, although since we have isolated many fewer clusters of this type, this is merely speculation. Indeed this is not the case for complexes **18–20**, the [Ni$_4$] and [Co$_4$] cubanes, where the deprotonated arm forms one corner of the cube and bridges to three metal centres with the remaining protonated arms bonding terminally. Thus each ligand adopts an $\eta^3,\eta^1,\eta^1,\mu_3$ mode and stabilises a triangular [M$_3$] unit.

Conclusions

The use of tripodal alcohols is an extremely successful way of synthesising polymetallic clusters that display high spin ground states and single-molecule magnetism behaviour. For all the complexes described the actual mechanism of formation will be a complicated process involving the oxidation/reduction, protonation/deprotonation and structural rearrangement of several species in solution. However the presence of (deprotonated) tripodal alcohols will favour the formation and isolation of elaborate polymetallic arrays comprising linked or fused [M$_3$] units. While this in itself is of course no guarantee that the cluster will show SMM behaviour, it should increase the likelihood of obtaining high spin molecules since the products will often display a degree of spin frustration and/or a number of competing exchange interactions of comparable magnitude that will prevent the spin alignments that may have otherwise been preferred. This 'rational serendipity' has indeed led to the isolation of several such Mn, Fe, Ni and Co clusters ranging in nuclearity from two to thirty-two.

This research is still in its infancy and thus the future promises many more new and exciting compounds with a host of new paramagnetic metals including other 3d transition metals, combinations of 3d with 4d, 5d and 4f metals and homometallic 4f clusters.

Acknowledgements

The work described has been done in collaboration with a number of groups. In particular, the author wishes to thank Prof. George Christou (University of Florida), Dr Wolfgang Wernsdorfer (Laboratoire Louis Néel), Drs David Collison and Eric McInnes (University of Manchester), Prof. Talal Mallah (Université Paris-Sud), Drs Guillem Aromí and Joan Cano (Universitat de Barcelona) and Prof. Hans Güdel (Universität Bern).

EKB would also like to thank Drs Leigh Jones, David Low, Stergios Piligkos and Gopalan Rajaraman for their invaluable contribution to this work.

Funding for the research was given by Lloyd's of London Tercentenary Foundation, The Leverhulme Trust and the EPSRC (UK).

References

1 (*a*) R. Sessoli, H.-L. Tsai, A. R. Schake, S. Wang, J. B. Vincent, K. Folting, D. Gatteschi, G. Christou and D. N. Hendrickson, *J. Am. Chem. Soc.*, 1993, **115**, 1804; (*b*) R. Sessoli and D. Gatteschi, *Angew. Chem., Int. Ed.*, 2003, **42**, 268.

2 See for example D. N. Hendrickson, G. Christou, H. Ishimoto, J. Yoo, E. K. Brechin, A. Yamaguchi, E. M. Rumberger, S. M. J. Aubin, Z. Sun and G. Aromí, *Mol. Cryst. Liq. Cryst.*, 2002, **376**, 301.

3 (*a*) M. N. Leuenberger and D. Loss, *Nature*, 2001, **410**, 789; (*b*) W. Wernsdorfer, N. Aliaga-Acalde, D. N. Hendrickson and G. Christou, *Nature*, 2002, **416**, 406; (*c*) S. Hill, R. S. Edwards, N. Aliaga-Alcade and G. Christou, *Science*, 2003, **302**, 1015; (*d*) J. Tejada, E. M. Chudnovsky, E. del Barco, J. M. Hernandez and T. P. Spiller, *Nanotechnology*, 2001, **12**, 181.

4 (*a*) A. L. Barra, D. Gatteschi and R. Sessoli, *Chem. Eur. J.*, 2000, **6**, 1608; (*b*) A. L. Barra, *Appl. Magn. Reson.*, 2001, **21**, 619; (*c*) A. Bouwen, A. Caneschi, D. Gatteschi, E. Goovaerts, D. Schoemaker, L. Sorace and M. Stefan, *J. Phys. Chem. B*, 2001, **105**, 2658; (*d*) D. Zipse, J. M. North, N. S. Dalal, S. Hill and R. S. Edwards, *Phys. Rev. B*, 2003, 68.

5 (*a*) A. Morello, O. N. Bakharev, H. B. Brom and L. de Jongh, *J. Magn. Magn. Mater.*, 2004, **1015**, 272; (*b*) A. Morello, O. N. Bakharev, H. B. Brom and L. J. de Jongh, *Polyhedron*, 2003, **22**, 1745; (*c*) D. Procissi, B. J. Suh, A. Lascialfari, F. Borsa, A. Caneschi and A. Cornia, *J. Appl. Phys.*, 2002, **91**, 7173; (*d*) R. M. Achey, P. L. Kuhns, W. G. Moulton, A. P. Reyes and N. S. Dalal, *Polyhedron*, 2001, **20**, 1745; (*e*) A. G. Harter, N. E. Chakov, B. Roberts, R. Achey, A. Reyes, P. Kuhns, G. Christou and N. S. Dalal, *Inorg. Chem.*, 2005, **44**, 2122.

6 (*a*) S. Carretta, E. Liviotti, G. Amoretti, R. Caciuffo, A. Caneschi and D. Gatteschi, *Phys. Rev. B*, 2002, 65; (*b*) R. Basler, C. Boskovic, G. Chaboussant, H. U. Güdel, M. Murrie, S. T. Ochsenbein and A. Sieber, *ChemPhysChem*, 2003, **4**, 910.

7 E. J. L. McInnes, E. Pidcock, V. S. Oganesyan, M. R. Cheesman, A. K. Powell and A. J. Thomson, *J. Am. Chem. Soc.*, 2002, **124**, 9219.

8 (*a*) T. Baruah and M. R. Pederson, *Int. J. Quantum Chem.*, 2003, **93**, 324; (*b*) J. Kortus, M. R. Pederson, T. Baruah, N. Bernstein and C. S. Hellberg, *Polyhedron*, 2003, **22**, 1871; (*c*) K. Park, M. R. Pederson, S. L. Richardson, N. Aliaga-Alcalde and G. Christou, *Phys. Rev. B*, 2003, 68; (*d*) E. Ruiz, J. Cano, S. Alvarez, A. Caneschi and D. Gatteschi, *J. Am. Chem. Soc.*, 2003, **152**, 6791.

9 G. Christou, *Polyhedron*, 2005, DOI: 10.1016/j.poly.2005.03.021, and references therein.

10 See for example (*a*) D. Gatteschi, R. Sessoli and A. Cornia, *Chem. Commun.*, 2000, 725; (*b*) S. L. Castro, Z. Sun, C. M. Grant, J. C. Bollinger, D. N. Hendrickson and G. Christou, *J. Am. Chem. Soc.*, 1998, **120**, 2997; (*c*) E. C. Yang, D. N. Hendrickson, W. Wernsdorfer, M. Nakano, L. N. Zakharov, R. D. Sommer, A. L. Rheingold, M. Ledezma-Giraud and G. Christou, *J. Appl. Phys.*, 2002, **91**, 7382; (*d*) M. Murrie, S. J. Teat, H. Stoeckli-Evans and H. U. Güdel, *Angew. Chem., Int. Ed.*, 2003, **42**, 4653.

11 J. J. Sokol, A. G. Hee and J. R. Long, *J. Am. Chem. Soc.*, 2002, **124**, 7656.

12 E. J. Schelter, A. V. Prosvirin and K. R. Dunbar, *J. Am. Chem. Soc.*, 2004, **126**, 15004.

13 (*a*) S. Osa, T. Kido, N. Matsumoto, N. Re, A. Pochaba and J. Mrozinski, *J. Am. Chem. Soc.*, 2004, **126**, 420; (*b*) C. M. Zaleski, E. C. Depperman, J. W. Kampf, M. L. Kirk and V. L. Pecoraro, *Angew. Chem., Int. Ed.*, 2004, **43**, 3912; (*c*) A. Mishra, W. Wernsdorfer, K. A. Abboud and G. Christou, *J. Am. Chem. Soc.*, 2004, **126**, 15648; (*d*) A. Mishra, W. Wernsdorfer, S. Parsons, G. Christou and E. K. Brechin, *Chem. Commun.*, 2005, 2086.

14 (*a*) N. Ishikawa, M. Sugita and W. Wernsdorfer, *J. Am. Chem. Soc.*, 2005, **127**, 3650; (*b*) N. Ishikawa, M. Sugita and W. Wernsdorfer, *Angew. Chem., Int. Ed.*, 2005, **44**, 2931.

15 See for example (*a*) T. Mallah, C. Auberger, M. Verdaguer and P. Veillet, *J. Chem. Soc., Chem. Commun.*, 1995, 61; (*b*) A. Scuiller, T. Mallah, M. Verdaguer, A. Nivorozkhin, J. L. Thiolence and P. Veillet, *New J. Chem.*, 1996, **20**, 1; (*c*) C. J. Milios, C. P. Raptopoulou, A. Terzis, F. Lloret, R. Vicente, S. P. Perlepes and A. Escuer, *Angew. Chem., Int. Ed.*, 2003, **43**, 210; (*d*) D. N. Hendrickson, G. Christou, H. Ishimoto, J. Yoo, E. K. Brechin, A. Yamaguchi, E. M. Rumberger, S. M. J. Aubin, Z. Sun and G. Aromí, *Polyhedron*, 2001, **20**, 1479.

16 Z. J. Zhong, H. Seino, Y. Mizobe, M. Hidai, A. Fujishima, S. Ohkoshi and K. Hashimoto, *J. Am. Chem. Soc.*, 2000, **122**, 2952.

17 (*a*) D. M. Low, L. F. Jones, A. Bell, E. K. Brechin, T. Mallah, E. Riviere, S. J. Teat and E. J. L. McInnes, *Angew. Chem., Int. Ed.*, 2003, **42**, 3781; (*b*) G. Rajaraman, J. Cano, E. K. Brechin and E. J. L. McInnes, *Chem. Commun.*, 2004, 1476; (*c*) M. Murugesu, M. Habrych, W. Wernsdorfer, K. A. Abboud and G. Christou, *J. Am. Chem. Soc.*, 2004, **126**, 4766.

18 M. I. Khan and J. Zubieta, *Prog. Inorg. Chem.*, 1995, **43**, 1.

19 (*a*) R. C. Finn and J. Zubieta, *J. Cluster Sci.*, 2000, **11**, 4; (*b*) K. Hegetschweiler, H. Schmalle, H. M. Streit and W. Schneider, *Inorg. Chem.*, 1990, **29**, 3625; (*c*) K. Hegetschweiler, H. Schmalle, H. M. Streit, V. Gramllicj, H. U. Hund and I. Erni, *Inorg. Chem.*, 1992, **31**, 1299; (*d*) M. Cavaluzzo, Q. Chen and J. Zubieta, *J. Chem. Soc., Chem. Commun.*, 1993, 131; (*e*) K. Hegetschweiler, D. Gatteschi, A. Cornia, L. Hausherr-Primo and V. Gramlich, *Inorg. Chem.*, 1996, **33**, 4414; (*f*) C. Boskovic, H. U. Gudel, G. Labat, A. Neels, W. Wernsdorfer, B. Moubaraki and K. S. Murray, *Inorg. Chem.*, 2005, **44**, 3181; (*g*) A. Cornia, A. C. Fabretti, P. Garrisi, C. Mortalo, D. Bonacchi, D. Gatteschi, R. Sessoli, L. Sorace, W. Wernsdorfer and A. L. Barra, *Angew. Chem., Int. Ed.*, 2004, **43**, 1136. The first reported examples of SMMs containing the related ligand triethanolamine (H_3tea, $[N(CH_2CH_2OH)_3]$) are: (*h*) B. Pilawa, M. T. Kelemen, S. Wanka, A. Geisselmann and A. L. Barra, *Europhys. Lett.*, 1998, **43**, 7; (*i*) L. M. Wittick, K. S. Murray, B. Moubaraki, S. R. Batten, L. Spiccia and K. J. Berry, *Dalton Trans.*, 2004, 1003; (*j*) M. Murugesu, W. Wernsdorfer, K. A. Abboud and G. Christou, *Angew. Chem., Int. Ed.*, 2005, **44**, 892.

20 (*a*) E. K. Brechin, M. Soler, J. Davidson, D. N. Hendrickson, S. Parsons and G. Christou, *Chem. Commun.*, 2002, 2252; (*b*) E. K. Brechin, M. Soler, G. Christou, J. Davidson, D. N. Hendrickson, S. Parsons and W. Wernsdorfer, *Polyhedron*, 2003, **22**, 1771; (*c*) S. Piligkos, G. Rajaraman, M. Soler, N. Kirchner, J. van Slageren, R. Bircher, S. Parsons, H.-U. Güdel, J. Kortus, W. Wernsdorfer, G. Christou and E. K. Brechin, *J. Am. Chem. Soc.*, 2005, **127**, 5572.

21 W. Wernsdorfer, *Adv. Chem. Phys.*, 2001, **118**, 99.

22 (*a*) E. K. Brechin, M. Soler, G. Christou, M. Helliwell, S. J. Teat and W. Wernsdorfer, *Chem. Commun.*, 2003, 1276; (*b*) G. Rajaraman, M. Murugesu, M. Soler, W. Wernsdorfer, M. Helliwell, S. J. Teat, G. Christou and E. K. Brechin, *J. Am. Chem. Soc.*, 2004, **126**, 15445.

23 A. J. Tasiopoulos, W. Wernsdorfer, K. Abboud and G. Christou, *Angew. Chem., Int. Ed.*, 2004, **43**, 6338.

24 A. J. Tasiopoulos, A. Vinslava, W. Wernsdorfer, K. A. Abboud and G. Christou, *Angew. Chem., Int. Ed.*, 2004, **43**, 2117.

25 M. Murugesu, W. Wernsdorfer, J. Raftery, G. Christou and E. K. Brechin, *Inorg. Chem.*, 2004, **43**, 4203.

26 S. R. Cooper and M. Calvin, *J. Am. Chem. Soc.*, 1977, **99**, 6623.

27 G. Rajaraman, E. C. Sañudo, M. Helliwell, S. Piligkos, W. Wernsdorfer, G. Christou and E. K. Brechin, *Polyhedron*, 2005, DOI: 10.1016/j.poly.2005.03.046.

28 H. Miyakasa, R. Clérac, W. Wernsdorfer, L. Lecren, C. Bonhomme, K.-i. Sugiura and M. Yamashita, *Angew. Chem., Int. Ed.*, 2004, **43**, 2801.

29 R. T. W. Scott, S. Parsons, M. Murugesu, W. Wernsdorfer, G. Christou and E. K. Brechin, *Chem. Commun.*, 2005, 2083.

30 R. T. W. Scott, S. Parsons, M. Murugesu, W. Wernsdorfer, G. Christou and E. K. Brechin, *Angew. Chem., Int. Ed.*, 2005, DOI: 10.1002/anie.200501881.

31 (*a*) M. Soler, W. Wernsdorfer, K. Folting, M. Pink and G. Christou, *J. Am. Chem. Soc.*, 2004, **126**, 2156; (*b*) E. C. Sañudo, W. Wernsdorfer, K. A. Abboud and G. Christou, *Inorg. Chem.*, 2004, **43**, 4137; (*c*) E. K. Brechin, E. C. Sañudo, W. Wernsdorfer, C. Boskovic, J. Yoo, D. N. Hendrickson, A. Yamaguchi, H. Ishimoto, T. E. Concolino, A. L. Rheingold and G. Christou, *Inorg. Chem.*, 2005, **44**, 502.

32 M. Moragues-Cánovas, E. Rivière, L. Ricard, C. Paulsen, W. Wernsdorfer, G. Rajaraman, E. K. Brechin and T. Mallah, *Adv. Mater.*, 2004, **16**, 1101.

33 A. L. Barra, A. Caneschi, A. Cornia, F. F. de Biani, D. Gatteschi, C. Sangregorio, R. Sessoli and L. Sorace, *J. Am. Chem. Soc.*, 1999, **121**, 5302.
34 (*a*) L. F. Jones, E. K. Brechin, D. Collison, M. Helliwell, T. Mallah, S. Piligkos, G. Rajaraman and W. Wernsdorfer, *Inorg. Chem.*, 2003, **42**, 6601; (*b*) L. F. Jones, D. M. Low, M. Helliwell, J. Raftery, D. Collison, G. Aromí, J. Cano, T. Mallah, W. Wernsdorfer, E. K. Brechin and E. J. L. McInnes, *Polyhedron*, 2005, in press.
35 R. H. Laye and E. J. L. McInnes, *Eur. J. Inorg. Chem.*, 2005, 2811.
36 (*a*) L. F. Jones, A. Batsanov, E. K. Brechin, D. Collison, M. Helliwell, T. Mallah, E. J. L. McInnes and S. Piligkos, *Angew. Chem., Int. Ed.*, 2002, **41**, 4318; (*b*) R. Carrasco, J. Cano, T. Mallah, L. F. Jones, D. Collison and E. K. Brechin, *Inorg. Chem.*, 2004, **43**, 5410.
37 M. Moragues-Cánovas, M. Helliwell, L. Ricard, E. Rivière, W. Wernsdorfer, E. K. Brechin and T. Mallah, *Eur. J. Inorg. Chem.*, 2004, 2219.
38 C. E. Talbot-Eeckelaers, *MPhil Thesis*, The University of Manchester, 2004.
39 G. Aromí, S. Parsons, W. Wernsdorfer, E. K. Brechin and E. J. L. McInnes, *Chem. Commun.*, 2005, DOI: 10.1039/b510097f.
40 (*a*) J. Ribas, A. Escuer, M. Monfort, R. Vicente, R. Cortes, L. Lezama and T. Rojo, *Coord. Chem. Rev.*, 1999, **195**, 1027; (*b*) S. S. Tandon, L. K. Thompson, M. E. Manuel and J. N. Bridson, *Inorg. Chem.*, 1994, **33**, 5555; (*c*) T. K. Karmakar, B. K. Ghosh, A. Usman, H.-K. Fun, E. Rivière, T. Mallah, G. Aromí and S. K. Chandra, *Inorg. Chem.*, 2005, **44**, 2391.
41 A. K. Boudalis, B. Donnadieu, V. Nastopoulos, J. Modesto Clemente-Juan, A. Mari, Y. Sanakis, J.-P. Tuchagues and S. P. Perlepes, *Angew. Chem., Int. Ed.*, 2004, **43**, 2266.
42 R. Shaw, I. S. Tidmarsh, R. H. Laye, B. Breeze, M. Helliwell, E. K. Brechin, S. L. Heath, M. Murrie, S. Ochsenbein, H.-U. Güdel and E. J. L. McInnes, *Chem. Commun.*, 2004, 1418.
43 Z. Sun, P. K. Grantzel and D. N. Hendrickson, *Inorg. Chem.*, 1996, **35**, 4414.